Random-manifold to random-periodic depinning of an elastic interface

S. Bustingorry,[1] A. B. Kolton,[1] and T. Giamarchi[2]
[1]*CONICET, Centro Atómico Bariloche, 8400 San Carlos de Bariloche, Río Negro, Argentina*
[2]*DPMC-MaNEP, University of Geneva, 24 Quai Ernest Ansermet, 1211 Geneva 4, Switzerland*
(Received 30 June 2010; revised manuscript received 26 August 2010; published 21 September 2010)

We study numerically the depinning transition of driven elastic interfaces in a random-periodic medium with localized periodic-correlation peaks in the direction of motion. The analysis of the moving interface geometry reveals the existence of several characteristic lengths separating different length-scale regimes of roughness. We determine the scaling behavior of these lengths as a function of the velocity, temperature, driving force, and transverse periodicity. A dynamical roughness diagram is thus obtained which contains, at small length scales, the critical and fast-flow regimes typical of the random-manifold (or domain wall) depinning, and at large length scales, the critical and fast-flow regimes typical of the random-periodic (or charge-density wave) depinning. From the study of the equilibrium geometry we are also able to infer the roughness diagram in the creep regime, extending the depinning roughness diagram below threshold. Our results are relevant for understanding the geometry at depinning of arrays of elastically coupled thin manifolds in a disordered medium such as driven particle chains or vortex-line planar arrays. They also allow to properly control the effect of transverse periodic boundary conditions in large-scale simulations of driven disordered interfaces.

DOI: 10.1103/PhysRevB.82.094202 PACS number(s): 64.60.Ht, 75.60.Ch, 05.70.Ln

I. INTRODUCTION

The dynamics of elastic manifolds in disordered media have been widely studied in relation with the physical properties of many systems. Magnetic[1–4] or ferroelectric[5–7] domain walls, contact lines of liquid menisci,[8,9] fluid invasion fronts in porous media,[10,11] and fractures[12–16] can be modeled as elastic interfaces or lines. Such lines would be flat if they were not under the usually unavoidable action of quenched disorder. Periodic systems such as charge-density waves (CDW),[17] vortex lattices in type-II superconductors[18–20] or Wigner crystals[21] can be also modeled as elastic manifolds embedded in random environments. This manifold is described by the displacements around the perfect periodic lattice that would exist in the absence of disorder. No matter how weak is the disorder,[22] in all these systems the competition between elasticity and disorder gives rise to rough structures and complex collective pinning phenomena with interesting universal features.

Of special interest is the response of this kind of systems to an external uniform field, able to drive the elastic manifold in a given direction. Concrete examples are applied magnetic fields on magnetic domain walls, applied electrical fields on ferroelectric domain walls, fluid pressure on contact lines, tension on fractures, electrical currents on vortex lattices in superconductors, and electrical fields on charge density waves and Wigner crystals. Indeed, such a probe would be rather trivial if not because of the presence of quenched impurities: disorder breaks the translation symmetry (though not in a statistical sense), making the otherwise uniform displacement of the manifold a complicated process involving many degrees of freedom. Whether the elastic bonds of the manifold break or support the tearing produced by the disorder, the resulting flow can be plastic or elastic respectively, and in both cases a rich disorder-induced out-of-equilibrium phenomena can emerge. To understand these phenomena it was shown to be more convenient to start by restricting the study to the more tractable elastic flow case.

Elastic *depinning* is one of the most prominent and better understood examples of collective pinning dynamic phenomena.[23,24] At zero temperature the external field must overcome a finite threshold f_c in order to force the pinned system to acquire a finite steady-state velocity v. Below the depinning threshold a finite velocity is only possible at a finite temperature by thermal activation due to the presence of many metastable states separated by energetic barriers. These barriers tend to diverge when decreasing the drive in the so-called *creep* regime,[25,26] strongly impeding the motion at low driving forces, and tend to vanish at f_c giving place to a *thermal rounding*[27] of the depinning transition. These collective transport phenomena are experimentally relevant since a finite velocity in this kind of systems corresponds to physical quantities (magnetization, or polarization for domain walls, voltage for superconductors, current for CDW) that can be readily measured.

From the statistical physics point of view the most remarkable feature of the far from equilibrium steady-state motion near the depinning threshold f_c at zero temperature is the existence of a well-defined nontrivial critical behavior. Just above the threshold the motion is jerky, characterized by forwardly moving avalanches of a typical size $\xi \sim (f-f_c)^{\nu}$ and width $w \sim \xi^{\zeta}$ produced at a typical rate $\tau \sim \xi^{z}$, yielding a mean velocity $v \sim (f-f_c)^{\beta}$, with $\beta = \nu(z-\zeta)$. ν, z, ζ are nontrivial characteristic exponents. These observations led to the fruitful analogy of the depinning transition with standard equilibrium critical phenomena, with v playing the role of the order parameter and f the role of the control parameter.[28] This analogy motivated an outburst of analytical and numerical work devoted to determine the value of critical exponents for different universality classes,[23,29–43] and to develop powerful analytical[44–46] and numerical[40,47–50] methods to obtain them. From the numerical viewpoint such a study requires a precise determination of the critical threshold f_c.[40]

For standard equilibrium phase transitions the low-temperature phase can be characterized by equilibrium correlation lengths separating the critical-looking short length

scales from the low-temperature fixed-point dominated large length scales. For the depinning transition it was shown that ξ also admits an analogous purely geometric interpretation as a crossover length in the average steady-state roughness of the (ordered) moving $v>0$ phase. The length ξ separates the regime of critical roughness at short length scales (i.e., with a roughness exponent of the critical configuration at f_c) from the fast-flow roughness observed at large length scales (i.e., with a roughness exponent identical to the strongly driven interface, $f \gg f_c$).[33,42,50] The steady-state geometry thus contains information of the velocity and there is no need to observe the transient correlated process of an avalanche. More recently, however, the analysis of the low-temperature averaged steady-state geometry has shown that no divergent steady-state correlation length scale exists approaching the threshold from below, thus breaking the naive analogy with standard phase transitions, where two divergent length scales are expected above and below the critical point.[49,50]

Elastic depinning universality classes were shown to depend on the dimension of the embedding space D, the dimension d of the manifold, or the number $N=D-d$ of displacement components of the manifold, the nature of the elastic interactions,[39,40,51,52] the anisotropy of the medium[53] and the nature of microscopic disorder correlations.[33,54] Considering for simplicity the case of d-dimensional directed manifolds with $N=1$ living in an isotropic uncorrelated disordered medium it is convenient to distinguish between two prominent groups, according to the correlations of the effective pinning force $F_p(u,\mathbf{r})$. This pinning force acts on the manifold displacement field $u(\mathbf{r})$, which measures the distance between the distorted and the perfectly flat manifold at the labeling point $\mathbf{r}$. On one hand the pinning force on interfaces such as domain walls or contact lines in random potentials usually display short-range correlations reflecting the fact that the interface sees a completely different disorder after shifting it a distance bigger than a certain characteristic finite width $r_f=\max[w,r_0]$, where w is the domain-wall width and r_0 the assumed finite correlation length of the disorder potential. We use random-manifold (RM) to denote this group, and we do not make distinction between the random-bond (RB) and random-field (RF) type of disorder since at depinning, unlike statics, they are known to merge into a single class.[33,48] Interfaces in periodic potentials or periodic condensates, such as charge density waves or periodic chains of elastically coupled objects, on the other hand display an effective pinning force with periodic correlations with a period M representing the period of microscopic potential in the first case and the lattice spacing in the second case. We use random-periodic (RP) to denote this group.

For short-range correlated isotropic disorder, the $N=1$ RM and RP classes have been traditionally studied, both numerically and analytically, using two paradigmatic models of disorder. While for modeling the large-scale dynamic behavior of a nonperiodic system it is enough to use any uncorrelated potential with range r_f, for modeling the periodic system the random-phase cosine potential have been traditionally chosen, thus forcing $M \sim r_f$. Although this is a good approximation for charge density waves (cf. Fukuyama-Lee-Rice model[55,56]), this kind of modeling does not permit however to study the interesting situation that can appear in different periodic systems for which the periodicity is much larger than the short-range correlation length of the disorder correlator, i.e., $r_f \ll M$. Indeed, when the autocorrelation of the pinning force is periodic and displays sharply localized peaks this physical situation, mostly analyzed for two component ($N=2$) displacement fields, was shown to be relevant for describing the statics of Wigner crystals[21,57] or vortex lattices,[58,59] where the lattice spacing a_0 can be made much larger than the vortex core size or coherence length ξ (cyclotron radius for Wigner crystals) by simply tuning an external magnetic field. In these cases the length-scale separation is responsible for the so-called RM regime of roughness. This regime occurs at intermediate length scales, before the system asymptotically reaches the so-called Bragg-glass or RP regime. Because the intermediate RM regime can span a wide range of lengths,[60,61] it can affect the static and dynamic properties of this kind of systems and thus can be experimentally observed. We can therefore expect additional geometrical crossovers around the depinning transition in these systems. From a numerical point of view, the effect of a periodicity $M \gg r_f$ in the critical depinning force distribution has been already analyzed in Ref. 62.

Here we present a study of the finite velocity dynamics of a simple RP system which includes localized periodic correlation peaks with controlled periodicity M, yielding an interesting multiscale behavior around depinning. Our main result is a geometrical dynamical roughness diagram which contains, at small length scales, the critical and fast-flow regimes typical of the RM (or "magnetic domain wall") depinning, and at large length scales, the critical and fast-flow regimes typical of the RP (or "charge-density wave") depinning. We argue that our results are qualitatively valid for the family of one-component periodic systems with localized correlations peaks, such as chains of elastically coupled thin interfaces. We compare, in particular, a driven chain of interacting particles in a one-dimensional disordered potential with an elastic line in disordered potential with periodic correlations at a larger scale. Our results are particularly relevant for properly controlling and interpreting the effect of periodic boundary conditions in large-scale simulations of driven interfaces.

Outline of the paper

The paper is organized as follows. In Sec. II we describe the general class of random periodic systems with localized periodic correlation peaks for which we argue our general results apply. Then, Sec. III presents the general properties of the structure factor, which will be used to analyze the geometry of rough interfaces. The main result of this work is the dynamical roughness diagram presented in Sec. IV based on scaling arguments. Section V gives the details of the performed numerical simulations that will be presented in Sec. VI and give support to the proposed dynamical roughness diagram. Then, in Sec. VII we will present a discussion of the RM-RP crossover, the relation between the elastic string and particle chain models, the extensions of the roughness diagram to the creep regime, and the implications of our results to numerical simulations with periodic boundary conditions. Finally, Sec. VIII presents the conclusions of the present work.

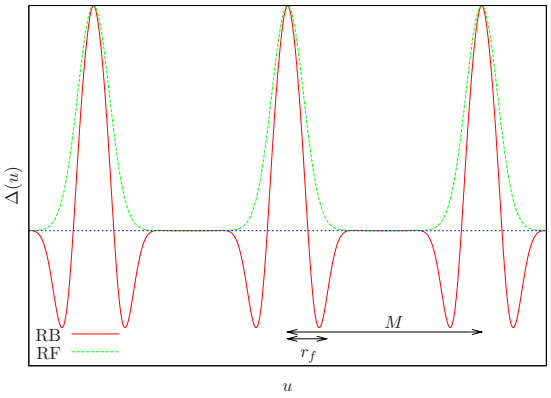

FIG. 1. (Color online) Schematic pinning force correlator for a random periodic system with periodicity M and localized correlation peaks with range r_f. RB and RF stand for random-bond and random-field correlations (see the text for details).

II. RANDOM PERIODIC SYSTEMS WITH LOCALIZED CORRELATION PEAKS

As a model for a random periodic system with well-separated length scales r_f and M we focus our study on directed elastic interfaces described by a one component displacement field $u(\mathbf{r},t)$ with internal dimension d, $\mathbf{r}\in\Re^d$, with $D=d+1$ the dimension of the embedding space, which satisfy an overdamped equation of motion

$$\gamma\partial_t u(\mathbf{r},t) = c\nabla^2 u(\mathbf{r},t) + F_p(u,\mathbf{r}) + f + \eta(\mathbf{r},t), \tag{1}$$

where γ is the friction coefficient, c the elastic constant, and the uniform external force is given by f. The thermal fluctuations satisfy

$$\langle \eta(\mathbf{r},t)\rangle = 0, \tag{2}$$

$$\langle \eta(\mathbf{r},t)\,\eta(\mathbf{r}',t')\rangle = 2\gamma T\delta(t-t')\,\delta(\mathbf{r}-\mathbf{r}'), \tag{3}$$

where the brackets correspond to thermal average. Therefore the system asymptotically relaxes to the canonical thermal equilibrium at temperature T in the absence of the driving force f. The pinning forces are characterized by sample-to-sample fluctuations given by

$$\overline{F_p(u,\mathbf{r})F_p(u',\mathbf{r}')} = \Delta(u-u')\,\delta(\mathbf{r}-\mathbf{r}'), \tag{4}$$

where the overbar indicates average over disorder realizations. In this paper we consider the case when the correlator function $\Delta(u)$ is a periodic function with correlation peaks localized in a range $r_f \ll M$ at the values $u=pM$ with M the periodicity and p any integer. We do not make a distinction between the so-called random bond, where we must enforce $\int du\Delta(u)=0$ and the random-field cases (see e.g., Ref. 33) since we are interested in the depinning transition where these two different static universality classes merge into a single one (in the creep regime, for $f<f_c$ and $T>0$ the distinction must be done however since the static properties can affect the intermediate length-scale physics[33,50]). In Fig. 1 we schematically represent the shape of $\Delta(u)$.

A periodic pinning force with fluctuations given by Eq. (4) arises naturally in numerical simulations of interfaces in random environments, when analyzing a system of transverse size M with periodic boundary conditions. We will exploit this fact to get most of our numerical results.

Interestingly, as we will show later, we find that the roughness scaling for elastic lines in a random-periodic two-dimensional potential with periodicity M in the direction of displacement also describe a chain of elastically coupled particles in a one-dimensional nonperiodic random potential with the lattice spacing given by M. We argue that this connection is general, between a d-dimensional elastic manifold in a random-periodic medium and a periodic chain of $(d-1)$-dimensional coupled manifolds. The dynamics of a discrete chain of d-dimensional coupled manifolds can be described by

$$\gamma\partial_t u_n(\mathbf{r},t) = \tilde{c}[u_{n+1}(\mathbf{r},t) + u_{n-1}(\mathbf{r},t) - 2u_n(\mathbf{r},t)] + c\nabla^2 u_n(\mathbf{r},t) + G_p(nM+u_n,\mathbf{r}) + F + \eta_n(\mathbf{r},t), \tag{5}$$

where u_n describes the displacements of each manifold around the perfect position nM in the chain, $\tilde{c}$ is a compression elastic constant, and $G(u,\mathbf{r})$ an uncorrelated pinning force which is the same, independently of n, with a *nonperiodic* short-range correlator of range r_f. In this case, the correlations of the thermal noise are given by $\langle \eta_n(\mathbf{r},t)\,\eta_m(\mathbf{r},t)\rangle = 2\gamma T\delta_{nm}\delta(\mathbf{r}-\mathbf{r}')\,\delta(t-t')$. The connection between the physics of Eq. (1) for d-dimensional manifolds and Eq. (5) for $d-1$-dimensional manifolds is subtle since it involves a nontrivial coarse graining in the direction of the periodicity which can produce extra terms in the equation of motion.[52,58,59] This issue will be discussed in more detail later. It is however plausible at this point that the resulting pinning force would display, *if* distortions are locally smooth, i.e., $|u_{n+1}-u_n| \ll M$, well-developed periodic correlations with a period M in the direction of the chain displacement with correlation peaks localized in a range $r_f \ll M$, as the ones schematically shown in Fig. 1.

III. ROUGH GEOMETRY AROUND DEPINNING

We focus our study on the geometrical observables that can be defined for the sliding manifold. The structure factor S_q is a very convenient quantity to study the geometry of the manifold at different length scales and to locate the different crossovers.[43,47,49,50,63,64] We define it as

$$S_q = \overline{\left\langle \left| \int e^{i\mathbf{q}.\mathbf{r}} u(\mathbf{r})\,d\mathbf{r} \right|^2 \right\rangle} \tag{6}$$

by choosing $\mathbf{q}=q\hat{x}$ in a particular direction x, corresponding to the direction of one of the internal dimensions if the interface is governed by Eq. (1), and corresponding to the direction of displacement (i.e., the direction of the chain) if it is described by Eq. (5).

The driven steady-state geometry at low temperatures is governed by three reference states:[49,50] the $f=0$ equilibrium state, the $f=f_c$ and $T=0$ depinning critical state, and the fast-flow state $f\to\infty$. The particularity of these states is that above a microscopic length they have different self-affine geometries, i.e., the structure factor behaves as

TABLE I. RM and RP characteristic roughness exponents for the three reference states: equilibrium (EQ), depinning (dep), and fast-flow (FF). In the static equilibrium case only the random-bond (RB) class is quoted.

$d=1$	RM	RP
EQ	$\zeta_{EQ}=2/3$(RB)	$\zeta_{EQ}^{RP}=1/2$
dep	$\zeta=1.25$	$\zeta^{RP}=3/2$
FF	$\zeta_{FF}=1/2$	$\zeta_{FF}^{RP}=3/2$

$$S_q \sim q^{-(d+2\zeta)}, \tag{7}$$

where the power-law behavior reflects the lack of a characteristic length scale in these states and ζ is the characteristic roughness exponent. The roughness exponents of the reference states are ζ_{EQ}, ζ, and ζ_{FF}, respectively. These exponents can take different values in different universality classes. While ζ_{EQ} is different for the RB, RF, and RP universality classes, ζ and ζ_{FF} remain the same for RB and RF classes and they change for the RP class. Since we are particularly interested in distinguishing the depinning and fast-flow roughness exponents of the RP class and the RM class, we use a superindex "RP" in all the exponent to indicate when the exponents belong to the RP case, and omit the superindex for the RM class (see Table I).

Furthermore, two important characteristic roughness exponents are the Larkin exponent ζ_L and the thermal exponent ζ_{TH}, which are, in general, expected to appear at very small length scales. The Larkin exponent is simply obtained by doing a first-order perturbation expansion in the disorder, thus replacing it by a random uncorrelated force. It yields $\zeta_L=(4-d)/2$ for lengths smaller than the Larkin length l_c, above which the naive perturbation theory fails due to metastability. The thermal roughness exponent $\zeta_{TH}=(2-d)/2$ is defined as the one that appears in absence of disorder at finite temperature and can be obtained exactly from the Edwards-Wilkinson equation.[65] Interestingly, we will show later that both, ζ_L and ζ_{TH} reappear at *large* length scales in the dynamics of a RP system with localized correlation peaks: $\zeta_{FF}=\zeta_{TH}$, $\zeta^{RP}=\zeta_{FF}^{RP}=\zeta_L$.

The steady-state geometry at small velocities can in general be described by velocity- and temperature-dependent crossover lengths separating different regimes of roughness. The corresponding roughness exponents are however universal, velocity and temperature independent, and coincide with one of the aforementioned exponents. For velocities just above the RM depinning transition we have

$$S_q \sim \begin{cases} q^{-(d+2\zeta)} & \text{for } q > 1/\xi \\ q^{-(d+2\zeta_{FF})} & \text{for } q < 1/\xi \end{cases} \tag{8}$$

allowing to define the characteristic length ξ. For small velocities and vanishing temperatures ξ can be identified with a velocity-dependent divergent correlation length $\xi \sim v^{-\nu/\beta}$. At $f \to f_c^+$ and zero temperature we have $\xi \sim (f-f_c)^{-\nu}$,[42] with $v \sim (f-f_c)^{\beta}$, and at $f=f_c$ and small temperatures we have $\xi \sim T^{\psi\nu/\beta}$,[43] with ψ a thermal rounding exponent such that $v \sim T^{\psi}$. Since in this case S_q is governed by a single crossover length ξ we can write the scaling form

$$S_q \sim \xi^{d+2\zeta} s(q\xi), \tag{9}$$

where the scaling function $s(x)$ behaves as $s(x) \sim x^{-(d+2\zeta_{FF})}$ for $x \ll 1$ and $s(x) \sim x^{-(d+2\zeta)}$ for $x \gg 1$. By plotting ξ vs v we can obtain a "geometrical roughness diagram" showing sectors with different roughness exponents at different observation length scales l: ζ for $l < \xi$ and ζ_{FF} for $l > \xi$. Physically, ξ divides the small length scales which are dominated by the critical configuration, i.e., the unique $v=0$ steady-state solution of the equation of motion for $f=f_c$, from the large length scales, which are governed by an effective Edwards-Wilkinson equation with a velocity-dependent effective temperature dynamically induced by the disorder.[33] The physical origin of this crossover is due to the fact that at small but finite velocity the renormalized disorder becomes a weak perturbation at large enough length scales, acting effectively as a thermal-like noise in an Edwards-Wilkinson equation, with a short-range correlation time of order r_f/v and effective strength or "temperature" $\Delta(0)/v$.

In a random-periodic system with localized correlation peaks, as the ones described in the previous section, the scaling of Eq. (9) must be corrected to take into account the existence of the additional characteristic distance M. As we show in the next section, M induces new geometrical crossovers at depinning, separating the geometrical roughness diagram in more than two sectors.

IV. DEPINNING ROUGHNESS DIAGRAM AND SCALING ARGUMENTS

In this section we summarize our most important physical results about the steady-state geometry of driven random-periodic systems with localized periodic correlation peaks. We present the depinning roughness diagram and heuristic scaling arguments describing the different crossovers. These arguments are corroborated numerically and analytically in the following sections.

In Fig. 2 we schematically show the geometric roughness diagram we find, by analyzing the structure factor, for a random periodic system with localized correlation peaks. It presents three roughness sectors, characterized by the roughness exponents of the RM depinning ζ, the RM fast flow ζ_{FF} and the RP fast flow ζ_{FF}^{RP}. Interestingly, unlike the RM case, for the RP system $\zeta^{RP}=\zeta_{FF}^{RP}$, and therefore there is no signature, in the steady-state structure factor, of the divergent length scale ξ_P expected for the depinning transition of a pure RP system. We discuss this issue later. Below a characteristic velocity v_P the system crosses over, at a characteristic velocity-independent length L_P, from a small length-scale regime with a roughness exponent ζ, corresponding to the geometry of the RM critical configuration, toward a regime with an exponent ζ^{RP}, corresponding to the RP critical configuration. Above v_P there are two crossovers, at the characteristic velocity-dependent length scales ξ and L_M. The first crossover is from a regime characterized by the RM critical depinning exponent ζ to a regime with the fast-flow RM exponent ζ_{FF}. The second crossover, observed by further in-

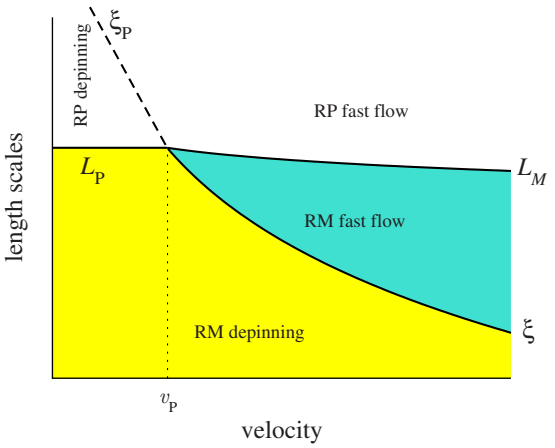

FIG. 2. (Color online) Schematic roughness diagram at the depinning transition of a random-periodic system with periodicity M and localized periodic correlation peaks as a function of its steady-state velocity v. For $v<v_P$, the geometry is of the RM (or domain-wall) class at small length scales $l<L_P$, while it is of the RP (or charge-density-wave) class at large length scales $l>L_P$, where $L_P \equiv L_P(M)$ but independent of the velocity v. For $v>v_P$, the geometry is of the RM class at small length scales $l<\xi$, where $\xi \equiv \xi(v)$ is the RM depinning correlation length. By further increasing the observation length-scale a crossover between RM and RP fast-flow regimes of roughness occurs at the length $L_M \equiv L_M(M,v)$. Note that the large scale geometry is described by only one roughness exponent since fast-flow and depinning exponents coincide in the RP class, $\zeta^{RP}=\zeta_{FF}^{RP}$. The proposed scaling with the velocity v and the periodicity M of the dynamical crossover lengths $\xi(v)$, $L_P(M)$, $L_M(v,M)$ (see text) is corroborated by analyzing the structure factor obtained from numerical simulations.

creasing the observation length scale, is from the RM fast-flow regime to the RP fast-flow regime, the latter characterized by the exponent ζ_{FF}^{RP} dominating the largest length scales.

The different length scales and roughness exponents shown in Fig. 2 can be obtained by analyzing the structure factor. To illustrate how we obtain the roughness diagram, in Fig. 3(a) we show a typical averaged structure factor for $v>v_P$ for an interface in a random periodic disorder medium with period M for parameters where we can identify the two crossovers in a single plot. The straight lines are here only indicative and correspond to the known roughness exponents ζ, ζ_{FF} and ζ_{FF}^{RP}, which are shown to be consistent with our numerical simulations. Increasing the observation length scale (decreasing the wave vector q) we see different crossovers between different roughness regimes at the characteristic length scales ξ and L_M. In Fig. 3(b) we also show a typical structure factor for an elastic chain with lattice spacing M moving in a one-dimensional disordered medium, displaying identical regimes of roughness. This supports the argued connection between the *geometrical* properties of periodic chains of manifolds with internal dimensions d in $d+1$-dimensional pure random media and single interfaces of internal dimension $d+1$ in $d+2$-dimensional random-periodic media.

The geometric roughness diagram for a RP system with localized correlation peaks is richer than for the RM system,

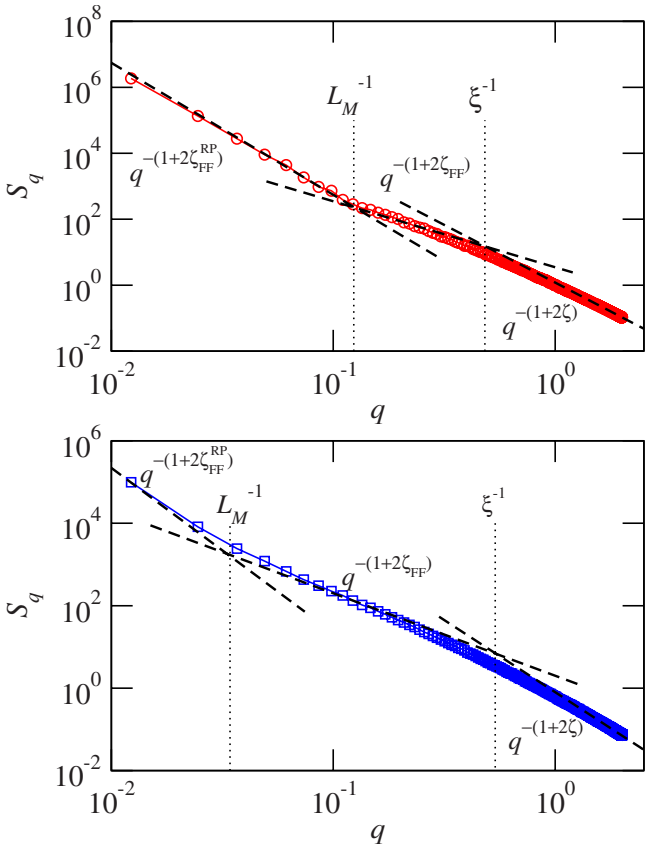

FIG. 3. (Color online) Typical structure factor for (a) a moving elastic string in a periodic random medium with periodicity M and (b) an elastic chain with lattice spacing M moving on a nonperiodic disorder medium. The velocity of these systems is larger than their characteristic velocity v_P (see Fig. 2). The two systems display a critical RM depinning roughness at small length scales which crosses over to a RM fast-flow roughness at intermediate length scales, and then to a RP fast-flow roughness at the largest length scales. These regimes are separated by two characteristic dynamical length scales: the correlation length ξ and the periodicity-induced length scale L_M.

which only displays one critical characteristic length scale ξ above f_c. This is due to the fact that M is an extra characteristic length in the problem, different from r_f, unlike what occurs in CDW systems. Interestingly, the RP system we study thus contains the RM depinning diagram, with its ζ and ζ_{FF} roughness sectors, for velocities larger than v_P and lengths below L_M. Indeed, we find $\xi \sim v^{\nu/\beta}$ (independent of the periodicity M) which coincides with the divergent length scale of the RM depinning, being ν and β RM critical exponents. We can thus say that below L_M for $v>v_P$ and below L_P for $v<v_P$ periodicity effects, both spatial and temporal, are not important. In other words, short lengths scales decorrelate rapidly, spatially and temporally, and cannot sense the periodic correlations of the pinning force.

To understand L_P we can make the simple scaling hypothesis that periodicity effects start to be important when the average transverse size or width of the critical manifold is of the order of the periodicity M, $w \sim M$. Since at small lengths l, the width grows as $w=r_f(l/l_c)^{\zeta}$ (both for $v<v_P$ and

$v > v_P$) we can compute the characteristic length L_P by stating that $M \sim r_f (L_P/l_c)^{\zeta}$. We thus obtain that

$$L_P \sim M^{1/\zeta} \tag{10}$$

independent of the velocity. This describes well our data as a function of M, v. Physically, L_P thus represents the length at which the critical configuration starts to see the periodic spatial correlations of the pinning force. Note that for the CDW case we have $M \sim r_f$ and thus $L_P \sim l_c$. Therefore we would not observe this RM critical sector for a CDW.

To estimate L_M for $v > v_P$ we must be more careful. Indeed, the static argument given above of matching the width w of the sliding manifold with M is incorrect in this case. This argument would give $M \sim r_f (\xi/l_c)^{\zeta} (L_M/\xi)^{\zeta_{FF}}$ or $L_M \sim \xi [(M/r_f)(l_c/\xi)^{\zeta}]^{1/\zeta_{FF}}$, and by using $\xi \sim v^{-\nu/\beta}$ we finally get $L_M \sim v^{-\nu(1-\zeta/\zeta_{FF})/\beta}$. Since, in general, $\zeta > \zeta_{FF}$ we get the incorrect result that L_M grows with the velocity, inconsistent with our data. The error in making such an argument comes from the fact that for $v > v_P$ the roughness of the interface is determined, above L_M, by the temporal correlations of the pinning force (when seen from the moving interface). Indeed, despite the fact that $w < M$ and that the renormalized disorder is already weak at L_M, periodicity effects are relevant above a certain length beyond which the manifold has not time to relax all its modes after moving by a distance M. The steady-state geometry of the moving system thus probes the periodic correlations of the pinning force. We must thus compare the typical relaxation time in the RM fast-flow regime $\tau(l) \sim \tau_c (\xi/l_c)^z (l/\xi)^{z_{FF}}$, for $\xi < l \leq L_M$, with the "time of flight" $\tau_M = M/v$, being $z_{FF} \equiv z_{TH} = 2$ the dynamical exponent of the fast-flow RM class, z the dynamical exponent of the critical RM regime, and τ_c a microscopic time. If these times equate at L_M

$$L_M \sim M^{1/z_{FF}} v^{-\chi} \tag{11}$$

with

$$\chi = \frac{1}{z_{FF}} - \frac{\nu}{\beta}\left(\frac{z}{z_{FF}} - 1\right). \tag{12}$$

This result with $\chi > 0$ describes well our numerical data, as we show later.

Having L_M and L_P we can now determine the characteristic velocity v_P of the roughness diagram, defined as $L_M(v_P) = L_P$. We get

$$v_P \sim M^{-1/\chi\zeta} \tag{13}$$

and therefore

$$L_M = L_P \left(\frac{v_P}{v}\right)^{\chi}. \tag{14}$$

It is worth noting here that while v_P decreases, L_M and L_P increase with increasing M. This means that for large enough M the RM sector of the roughness diagram of Fig. 2 grows and in practice the system behaves as a RM system. Conversely, for small M the RP sector grows and dominates the behavior at small velocities.

We also note that below v_P and above L_P we expect to observe RP or CDW-like depinning with a divergent correlation length $\xi_P \sim (f - f_c)^{-\nu^{RP}}$. However, unlike the RM case, the divergent length does not manifest itself as a crossover between roughness regimes of the structure factor, since $\zeta^{RP} \equiv \zeta_{FF}^{RP}$. This is consistent with the fact that the roughness exponent $\zeta^{RP} = \zeta_L = (4-d)/2$ for the RP appears in functional renormalization group calculations from the generation of a random force in the renormalized pinning correlator.[29] In other words, the pinning forces acting on pieces of size L_P are essentially uncorrelated and the model thus effectively becomes the Larkin model with a roughness exponent $\zeta_L = (4-d)/2$. In this respect, in Sec. VI we show that $\zeta_{FF}^{RP} \equiv \zeta_L$ from numerical simulations.

The roughness diagram of Fig. 2 appears to be valid at small finite temperatures within the "thermal-rounding" regime, as we find numerically. In this regime the effect of the temperature translates into a finite velocity $v \sim T^{\psi}$ at $f = f_c$ but does not affect the large-scale roughness regimes. The depinning roughness diagram of Fig. 2 thus remains the same, whether the velocity is originated by driving force, small temperature or both. In the following sections we describe our numerical simulation method and results supporting the roughness diagram of Fig. 2 and the scaling for the different crossover lines.

V. DETAILS OF NUMERICAL SIMULATIONS

We present here a detailed description of the numerical methods we use to study the RP system with localized correlation peaks. For simplicity we analyze low dimensional manifolds but our results remain qualitatively the same for higher dimensions. The $d=1$ case turns out to be on the other hand the most stringent case for our general arguments.

We study the motion of an elastic string in a disordered environment described by Eq. (1) in $d=1$ ($D=2$). In order to numerically solve Eq. (1) for the elastic string we discretize the $D=2$ embedding medium in the longitudinal z direction in L segments of unit size, keeping the transverse displacement field $u(z)$ as a continuous variable in the x direction. The discrete system of equations read

$$\gamma \partial_t u(z,t) = c[u(z+1,t) + u(z-1,t) - 2u(z,t)] + F_p(u,z) + f + \eta(z,t) \tag{15}$$

with z an integer. Periodic boundary conditions of size M (resp. L) are imposed for the transverse (respectively, longitudinal) system sizes. Besides avoiding boundary effects, this model presents several advantages which have been exploited in various ways for nonperiodic systems.[42,43,47,49,63] The critical force and critical configuration for such finite systems can be determined for each sample in polynomial time with arbitrary precision by exploiting the Middleton theorems.[39] Moreover, the complete sequence of metastable states below threshold, and, in particular, the one dominating the creep motion at low temperatures can be determined for each particular sample exactly, by generalized, Middleton-type, theorems.[49,50] This method thus allows for a well controlled analysis of key properties such as the critical force statistics, the critical exponents of the depinning transition, and the different roughness crossovers.

To show the generality of our results we also study for comparison the problem of an elastic chain by solving Eq. (5) in $D=1$ and $d=0$

$$\gamma\partial_t u_n(t) = \tilde{c}[u_{n+1}(t) + u_{n-1}(t) - 2u_n(t)] + G_p(nM + u_n) + f + \eta_n(t). \quad (16)$$

As mentioned above, Fig. 3 shows that the elastic string, described by Eq. (15) and the elastic chain, described by Eq. (16) display the same roughness crossovers around depinning. We argue that this geometrical equivalence is general, between the d dimensional manifold in a $D=d+1$ disordered medium with period M and the periodic chain of $d-1$ dimensional elastically coupled manifolds with lattice spacing M in a $D=d$ dimensional disorder medium. Therefore we study in details the case of the elastic string and translate appropriately our results to both kinds of systems in any dimension d. The resulting discrete system of equations for the elastic chain in $D=1$, Eq. (16) are indeed similar to the ones for the string in $D=2$, by identifying the discrete values of z for the particles of the string with the index n for the particles of the chain. The main differences between the two systems are the pinning force correlations. While the pinning force on the string is uncorrelated for different values of the labeling variable z, the pinning force on the chain is correlated for different values of the labeling variable n, since in the latter case the particles visit the same disorder as they move. This difference can be better appreciated by remarking that the equations for the elastic chain are equivalent (by interpreting n as z) to the ones of a tilted elastic string in a $D=2$ medium with columnar disorder, being $\theta=\tan^{-1}(M/L)$ the imposed tilting angle. The result of Figs. 3 is thus nontrivial and suggests that the roughness diagram of Fig. 2 is general for elastic system with pinning forces displaying localized disorder correlation peaks.

The equations of motion, Eqs. (15) and (16), are integrated using Euler method with a time step $\delta t=0.01$. We set $\gamma=1$, $c=\tilde{c}=1$, $r_f=1$, and a disorder strength $\Delta(0)=1$. A different choice of these microscopic parameters does not qualitatively alter our results. The continuous random potential for the string $V(u,z)=-\int du F_p(u,z)$ is modeled by L cubic splines passing through M regularly spaced uncorrelated Gaussian numbers points. For the chain, the potential $\tilde{V}(u)=-\int du G_p(u)$ is numerically generated with random spline passing through $L\times M$ regularly spaced uncorrelated Gaussian numbers points. Disorder average is done by averaging over different realization of the Gaussian random points. Using these disorder potential models, when $M \gg r_f$ the corresponding pinning forces display periodic correlations with localized peaks in a range r_f.

VI. NUMERICAL RESULTS

In this section we show and discuss the numerical results for the characteristics lengths, roughness exponents and characteristic velocities, appearing in the geometrical roughness diagram of Fig. 2. We describe separately the different crossovers for $v > v_P$ and $v < v_P$.

A. Roughness crossovers for $v > v_P$

We start by discussing the two crossovers observed in Figs. 3(a) and 3(b) for $v > v_P$, at the characteristic lengths ξ and L_M, respectively. One observes three roughness regimes for given values of L and M. They correspond to the three regimes observed in Fig. 2 for velocities above v_P. Increasing the length scale (decreasing the wave vector q) the local roughness exponent changes from $\zeta \approx 1.25$, to $\zeta_{FF}=0.5$, and finally to $\zeta_{FF}^{RP}=\zeta_L=1.5$. The first two roughness exponents are characteristic of the RM depinning and we can identify the crossover length ξ with the divergent correlation length of the RM depinning down to v_P. The second crossover length L_M is proper to our system, separating the fast-flow regime of the RM class from the one of the RP class.

For pure RM models the value $\zeta \approx 1.25$ was obtained numerically before by very different methods[66,67] and, in particular, by exact algorithms.[41,42] Two loop renormalization group calculations for the RM class are required to get values that are consistent with this result.[29] The exponent ζ_{FF} was obtained by numerical simulations,[42] and by analytical arguments.[33] As described above the physical meaning of the appearance of ζ_{FF} is that at large length scales the velocity v becomes very important and disorder effectively acts as an spatially uncorrelated time-dependent perturbation with short-range temporal correlations in a range r_f/v. The strength or "effective temperature" of this effective noise is thus proportional to $\Delta(0)/v$.[33] Eq. (1) then effectively becomes an Edwards-Wilkinson equation for which it is straightforward to show that the steady-state roughness exponent is $\zeta_{TH}=(2-d)/2$ for $d \leq 2$, and $\zeta_{TH}=0$ for $d>2$. For $d=1$ we have $\zeta_{FF}=\zeta_{TH}=1/2$, consistent with our numerical result for the present system.

As described in Sec. IV the crossover at L_M for $v > v_P$ occurs when the relaxation time of the string in the RM fast-flow regime becomes of the order of the time of flight M/v. The resulting scaling of L_M with M and v involves several exponents of the RM class, and hence it is a good test for the validity of our scaling arguments. For fixed external force and temperature and changing the transverse size M only the crossover around L_M changes in the structure factor, as observed in Figs. 4(a) and 5(a). Thus, for the crossover at large length scales the structure factor can be written, for $q \ll \xi^{-1}$ as

$$S_q L_M^{-(1+2\zeta_{FF})} = G(qL_M) \quad (17)$$

with $G(x) \sim x^{-(1+2\zeta_{FF}^{RP})}$ for $x \ll 1$ and $G(x) \sim x^{-(1+2\zeta_{FF})}$ for $x \gg 1$. Using Eq. (11) for L_M, and since the velocity is fixed by f and T, we get the following scaling formula

$$S_q M^{-(1+2\zeta_{FF})/z_{FF}} \sim G(qM^{1/z_{FF}}). \quad (18)$$

In Figs. 4(b) and 5(b) we test this scaling prediction as a function of M for a fixed velocity by plotting $S_q M^{-(1+2\zeta_{FF})/z_{FF}}$ vs $qM^{1/z_{FF}}$ for different values of M. In Fig. 4 the velocity is produced by a force above threshold at zero temperature while in Fig. 5 the velocity is produced by a finite but small temperature at $f=f_c$. In both cases we find that the scaling form proposed collapses well the different curves by using $z_{FF}=2$ which corresponds to the dynamical exponent of a

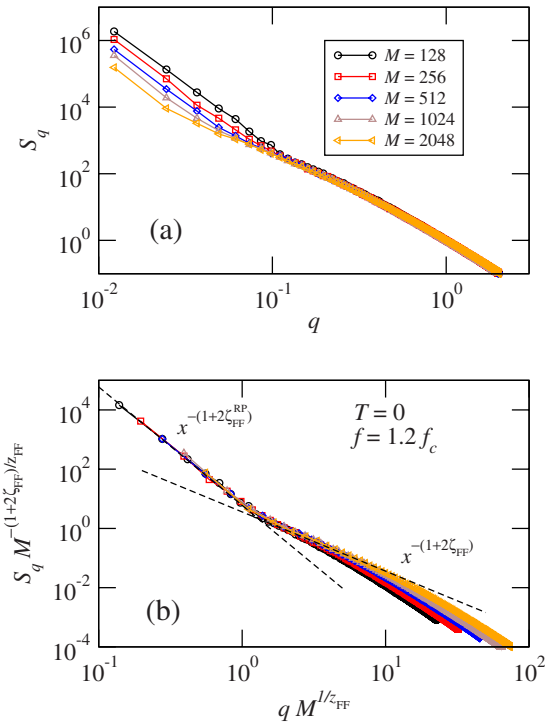

FIG. 4. (Color online) Scaling of the structure factor for different M values at $T=0$ and $f=1.2f_c$. The longitudinal system size is $L=512$. (a) Raw data. (b) Scaled data.

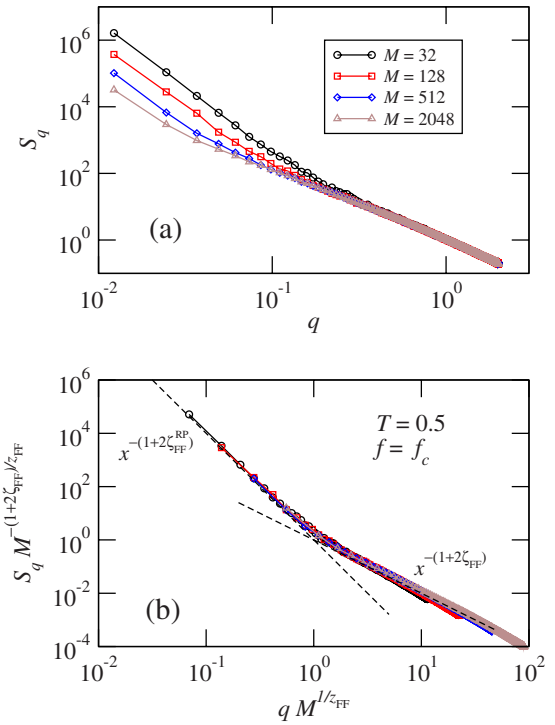

FIG. 5. (Color online) Scaling of the structure factor for different M values at $f=f_c$ and $T=0.5$. The longitudinal system size is $L=512$. (a) Raw data. (b) Scaled data.

RM model at large velocities (i.e., the dynamical exponent of the Edwards-Wilkinson equation with the disorder-induced Langevin-type noise). As expected, deviations from the good collapse are observed only at large q, where the presence of the extra characteristic length ξ invalidates the simple scaling of Eq. (18). We also note that in the nonscaled data in Figs. 4(a) and 5(a) S_q becomes M independent for $q \gg \xi^{-1}$. This is consistent with the fact that ξ does not depend on M but only on the velocity, $\xi \sim v^{-\nu/\beta}$ near depinning, unlike L_M which depends on both, v and M.

In order to study the velocity dependence of the structure factor and its crossover lengths we have applied both different driving forces $f \gtrsim fc$ at $T=0$ and small temperatures for $f=f_c$. In Figs. 6(a) and 7(a) we show S_q as a function of the force and temperature, respectively. The crossover around ξ can be described, for $q \gg L_M^{-1}$, with the scaling relation

$$S_q \sim v^{-(1+2\zeta)\nu/\beta} \tilde{G}[q v^{-\nu/\beta}] \tag{19}$$

with the function $\tilde{G}(x) \sim x^{-(1+2\zeta_{FF})}$ for $x \ll 1$ and $\tilde{G}(x) \sim x^{-(1+2\zeta)}$ for $x \gg 1$. This scaling form depends on force and temperature only through v. To get explicitly these dependencies we can use, for small v and $f \gtrsim f_c$ that $v \sim \tilde{f}^{\beta}$ for $f \gtrsim f_c$, with $\tilde{f}=(f-f_c)/f_c$ the reduced force, and $v \sim T^{\psi}$ for $f=f_c$ and small T.[43] Figures 6(b) and 7(b) show the respective scaling forms around ξ. However, this scaling form is valid up to the scale L_M where periodicity effects are important and $\tilde{G}(x)$ is not longer universal. The crossover of $\tilde{G}(x)$ to RP fast flow can be written as

$$\tilde{G}(x) \sim x_M^{-(1+2\zeta_{FF})} \bar{G}\left(\frac{x}{x_M}\right), \tag{20}$$

where $x_M = v^{-\nu/\beta}/L_M$ and the new function $\bar{G}(y) \sim y^{-(1+2\zeta_{FF}^{RP})}$ for $y \ll 1$ and $\bar{G}(y) \sim y^{-(1+2\zeta_{FF})}$ for $y \gg 1$. Using Eq. (11) one can write, for fixed M and for $q \ll 1/\xi$ that the structure factor behaves as

$$S_q \sim v^{-\kappa} \bar{G}(q v^{-\chi}) \tag{21}$$

with

$$\kappa = 2(\zeta - \zeta_{FF})\nu/\beta + (1 + 2\zeta_{FF})\chi. \tag{22}$$

This form describes the crossover between RM and RP fast-flow regimes of the structure factor. Figures 6(c) and 7(c) show this scaling form when the velocity is generated by finite drive at zero temperature or by a small finite temperature at $f=f_c$.

Therefore, in Figs. 6 and 7 we test the latter scaling prediction as a function of f for $f>f_c$ and $T=0$, and as a function of T for $f=f_c$ by using the known values $\beta=1/3$,[29,42] $\psi=0.15$.[43] Since S_q has two characteristic lengths L_M and ξ, we show separately the collapse around the two crossovers. In Figs. 6(b) and 7(b) we show the collapse around ξ and in Figs. 6(c) and 7(c) the collapse around L_M, for the same set of curves $S_q(f,T)$ of Figs. 6(a) and 7(a), respectively. The collapse obtained by using the known values of ψ, β ζ, ζ_{FF}, z, and z_{FF} fully supports our interpretation of the two crossovers.

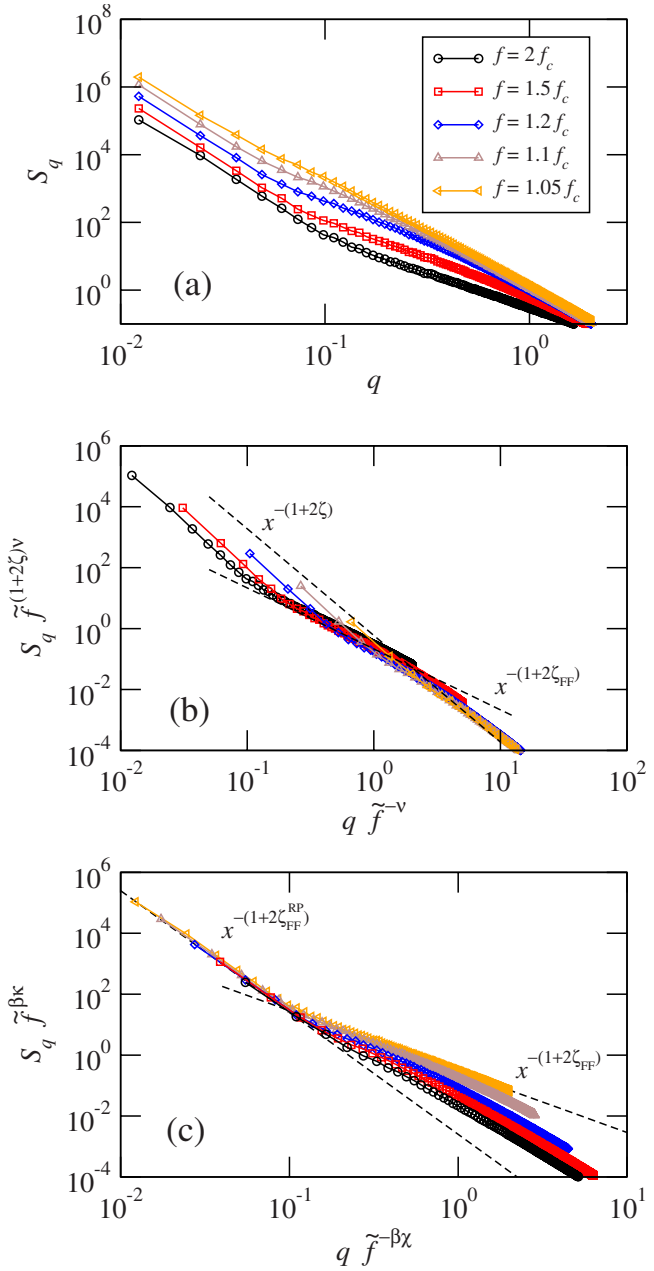

FIG. 6. (Color online) Scaling of the structure factor for different $f > f_c$ values at $T=0$ and $M < L^{\zeta}$. The longitudinal system size is $L=M=512$. (a) Raw data, (b) scaled data around ξ, and (c) scaled data around L_M.

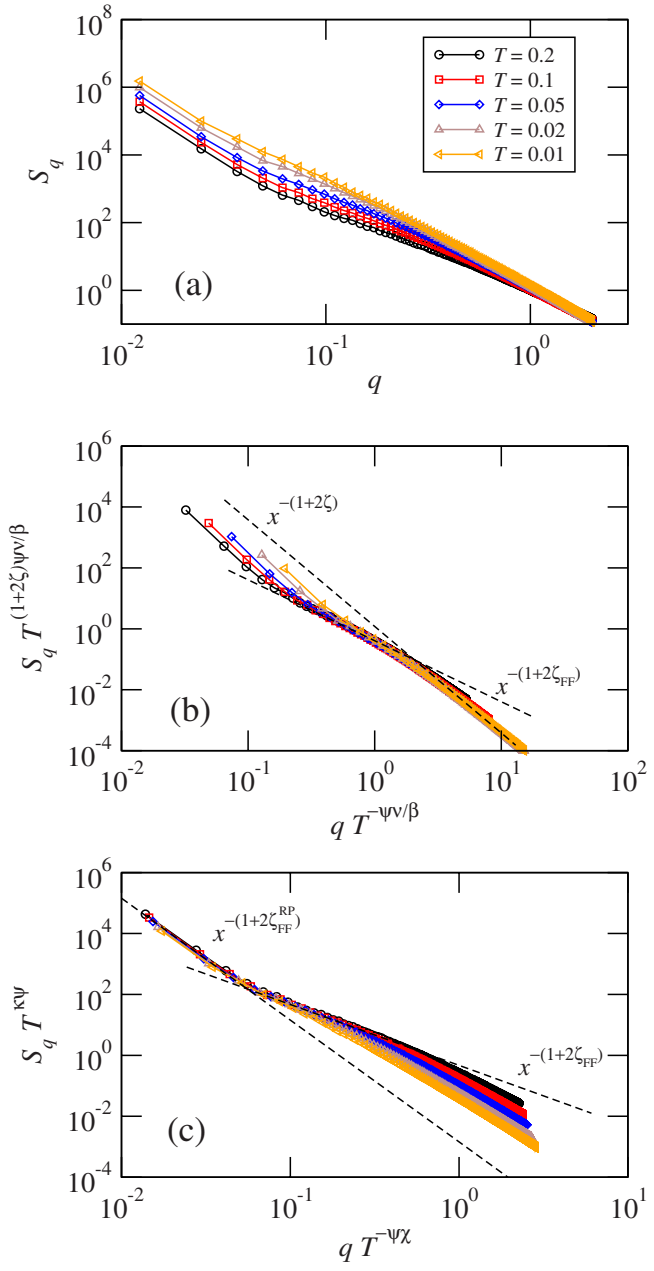

FIG. 7. (Color online) Scaling of the structure factor for different $T > 0$ values at $f = f_c$ and $M < L^{\zeta}$. The longitudinal system size is $L=M=512$. (a) Raw data, (b) scaled data around ξ, and (c) scaled data around L_M.

B. Roughness crossovers for $v < v_P$

As shown in Fig. 2, at v_P we have $L_M(v_P) = \xi(v_P) = L_P$, where L_P is independent of the velocity. The RM fast-flow regime thus disappears at v_P. This implies that periodicity effects are already generated by static pinned configurations and not dynamically as described in the derivation of L_M. L_P is precisely the length at which, for $v < v_P$, the width of a typical RM critically pinned configuration reaches M. Below L_P, periodicity effects are absent and the typical critical configuration is not sensitive to M. Just above L_P, the critical configuration crosses over to the RP class. To prove the existence of this crossover we show in Fig. 8 that the structure factor of a string with $L \gtrsim L_P$ and $v < v_P$ can be written as

$$S_q M^{-(1+2\zeta^{RP})/\zeta} = H(qM^{1/\zeta}) \tag{23}$$

with $H(x) \sim x^{-(1+2\zeta^{RP})}$ for $x \ll 1$ and $H(x) \sim x^{-(1+2\zeta)}$ for $x \gg 1$. We have used $L_P \sim M^{1/\zeta}$ and the previously known values of ζ^{RP} and ζ. The collapse of Fig. 8 thus supports our interpretation of this crossover.

As discussed in Sec. IV and shown in Fig. 2, we expect a second crossover at a length ξ_P above L_P, representing the dynamical correlation of the RP depinning. The regime between L_P and ξ_P thus represents the RP critical regime with

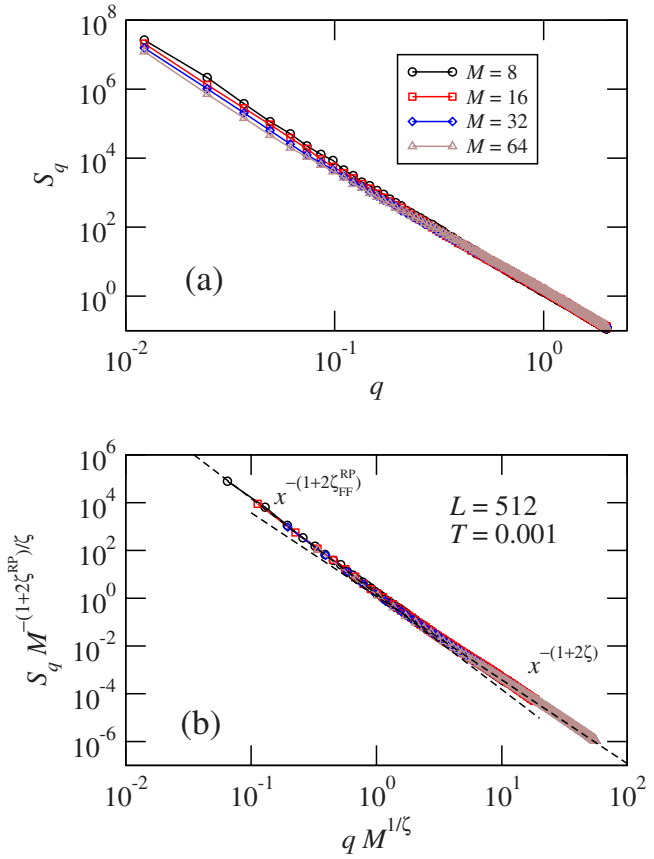

FIG. 8. (Color online) Scaling of the structure factor for different M values in the $v<v_P$ regime. Data correspond to $T=0.001$ and $L=512$. (a) Raw data. (b) Scaled data.

the roughness exponent of the RP critical configurations. As discussed in Sec. IV, $\zeta^{RP}=\zeta_{FF}^{RP}$, and due to the RP depinning correlation length ξ_P cannot be detected by analyzing S_q. This suggests that subtle geometrical measures are probably needed to locate ξ_P.[68]

VII. DISCUSSION

In this section we discuss, by analytical arguments and additional numerical simulations, the results obtained in the previous sections. We first discuss, in Sec. VII A, how to analytically calculate the crossover from random-manifold to random-periodic fast flow regimes of roughness at the length scale L_M, which is absent in the pure Random-Manifold or Random-Periodic depinning. The numerical results of Sec. VI support the depinning roughness diagram of Fig. 2 which is found to be the same for interface pinning potentials with periodic correlations and for periodic elastic systems such as chains. In Sec. VII B we discuss this interesting equivalence between the geometry of periodic elastic systems in random pinning potentials and interfaces in random-periodic pinning potentials. We give analytical and numerical arguments. In Sec. VII C we discuss how to extend the roughness diagram of Fig. 2 to the creep regime in the low temperature limit, based on the effects of periodicity in the statics and depinning. Finally, in Sec. VII D we discuss the implications of the roughness phase diagram for numerical simulations of elastic strings with periodic boundary conditions and the thermodynamic limit.

A. Random-manifold to random-periodic crossover in the fast flow regime

We show here how the crossover from random-manifold to random-periodic fast flow and their respective roughness exponents can be analytically computed. We consider here a simplified model of disorder perturbatively in the large velocity and small temperature limit of Eq. (15). We will show this approach yields correct results for the velocity and periodicity dependence of the crossover length, which can be therefore identified with L_M in Fig. 2, when using the renormalized friction, disorder strength and temperature at the length scale ξ.

At high velocities and small temperatures, we approximate the pinning force $F_p(u,\mathbf{r})$ by $F_p(vt,\mathbf{r})$. In doing so, we assume, *a priori*, that the disorder-induced and thermally induced displacements are small in the regime we are interested in. In this approximation the pinning force becomes an effective thermal-like noise $\tilde{\eta}(t,\mathbf{r})\equiv F_p(vt,\mathbf{r})$ with temporal correlations given by

$$\overline{\tilde{\eta}(t,\mathbf{r})\tilde{\eta}(t',\mathbf{r}')}=\Delta[v(t-t')]\delta(\mathbf{r}-\mathbf{r}'). \tag{24}$$

Since $\Delta(x)$ has a spatial range r_f, the range of temporal correlations of $\tilde{\eta}$ is r_f/v and its effective temperature proportional to $\Delta(0)/\gamma v$. Within this approximation, the equation of motion becomes linear, and its solution in Fourier space is, for a particular component $q=\mathbf{q}.\hat{z}$ of the wave vector $\mathbf{q}$

$$u_q(t)=\gamma^{-1}\int_0^t dt' e^{-cq^2(t-t')/\gamma}[f\delta_{q,0}+\tilde{\eta}_q(t)+\eta_q(t)]. \tag{25}$$

The instantaneous structure factor is thus given by

$$S_q(t)=\overline{\langle|u_q(t)|^2\rangle}=S_q^{EW}(t)+S_q^{FF}(t), \tag{26}$$

where the first contribution is the Edwards-Wilkinson or purely thermal structure factor

$$S_q^{EW}(t)=\frac{T}{cq^2}(1-e^{-2cq^2t/\gamma}) \tag{27}$$

and the second contribution comes from the disorder-induced noise $\tilde{\eta}$

$$S_q^{FF}(t)=\gamma^{-1}\int_0^t\int_0^t dt_1 dt_2 e^{-cq^2(2t-t_1-t_2)/\gamma}\Delta[v(t_2-t_1)]. \tag{28}$$

To proceed we assume a particular periodic correlator $\Delta(u)=\Delta(u+nM)$ with n an integer. A simple choice for $\Delta(u)$ having sharply localized peaks at $u=nM$ is

$$\Delta(u)=\Delta_p\sum_n \delta(u-nM). \tag{29}$$

This kind of disorder arises physically from a random distribution of identical point like pinning centers acting on a very

thin interface, in the limit $r_f \to 0$ with the constraint $\int_0^M dx\Delta(x)=\Delta_p$ and Δ_p a constant measuring the strength of the disorder. With such disorder the fast-flow contribution to the structure factor can be easily integrated to get

$$S_q^{\mathrm{FF}}(t) = \frac{\Delta_p}{2\gamma v c q^2}(1-e^{-2cq^2 t/\gamma})\frac{1}{1-e^{-2cq^2 M/\gamma v}}. \quad (30)$$

Then, the total instantaneous structure factor can be expressed as

$$S_q(t) = S_q^{\mathrm{EW}}(t)\left(1+\frac{\Delta_p}{2\gamma v T}\frac{1}{1-e^{-2cq^2 M/\gamma v}}\right). \quad (31)$$

Since we are interested in the steady-state we take the $t\to\infty$ limit to obtain the steady-state structure factor

$$S_q = \frac{1}{cq^2}\left(T+\frac{\Delta_p}{2\gamma v}\frac{1}{1-e^{-2(ql_M)^2}}\right), \quad (32)$$

which presents the characteristic length $l_M \equiv \sqrt{Mc/\gamma v}$ or characteristic time $\tau_M \equiv M/v$.

For large length scales such that $q \ll l_M^{-1}$ we have

$$S_q \approx \frac{T}{c}q^{-2}+\frac{\Delta_p}{4cM}q^{-4}, \quad (33)$$

where the velocity v does not appear explicitly. At $T=0$, $S_q \sim q^{-4}$, implying that the large scale roughness exponent is identical to the one of the Larkin model $\zeta_{\mathrm{L}}=(4-d)/2$ if $d \leq 4$ and $\zeta_{\mathrm{L}}=0$ otherwise. This is consistent with our finding $\zeta_{\mathrm{FF}}^{\mathrm{RP}}=\zeta_{\mathrm{L}}=3/2$ for the $d=1$ case (string) in a random periodic medium and also for the elastic chain. If $T>0$ we could have a roughness crossover at $q_T=\sqrt{\frac{\Delta_p}{4TM}}$, where the two terms in Eq. (33) become equal. However, for this roughness crossover between ζ_{TH} (with $\zeta_{\mathrm{TH}}=(2-d)/2$ for $d\leq 2$ and $\zeta_{\mathrm{TH}}=0$ otherwise) to ζ_{L} to be observable we must require $q_T \ll l_M^{-1}$ or equivalently $T \gg \Delta_p c/v$. Since Δ_p/v can be identified with the shaking temperature T_{sh} of Ref. 69 the condition for observing this crossover in this regime reads $T_{sh}(v) \ll T$, meaning that disorder-induced fluctuations must be much smaller than thermal fluctuations.

If $q \gg l_M^{-1}$ on the other hand, we have

$$S_q \approx \frac{1}{cq^2}\left(T+\frac{\Delta_p}{2v}\right), \quad (34)$$

which is equivalent to the Edwards-Wilkinson structure factor at an effective temperature $T_{\mathrm{eff}}(v)=T_{\mathrm{sh}}(v)+T$, yielding a roughness exponent ζ_{TH}.

From Eqs. (34) and (33) we thus see that if the temperature is small compared to $T_{\mathrm{sh}}(v)=\Delta_p/2v$ there is a roughness crossover at the length scale l_M from $\zeta_{\mathrm{FF}}=\zeta_{\mathrm{TH}}$ to $\zeta_{\mathrm{FF}}^{\mathrm{RP}}=\zeta_{\mathrm{L}}$ when increasing the observation length scale. This is in agreement with the roughness diagram of Fig. 2 for $v>v_{\mathrm{P}}$ and lengths above ξ. By comparing l_M and L_M we see that both quantities have the same M dependence, since $z_{\mathrm{FF}}=2$. The explicit velocity dependence, even if it is a power law in both cases, is different. In this model we find $l_M \sim (\gamma v)^{-1/2}$, instead of $L_M \sim v^{-1/2+(\nu/\beta)(z/2-1)}$ which describes well our data and was predicted in Eq. (11) by pure scaling arguments. We also note in this respect that the structure factor at small q predicted by the model appears to be velocity independent and temperature dependent, in contrast to what we predict by scaling arguments and what the data presented in Sec. VI supports. These differences can be directly attributed to the incorrect use of the bare friction constant γ, disorder strength Δ_p, and temperature T in our perturbation theory, instead of using their renormalized velocity-dependent values $\tilde{\gamma}(v)$, $\tilde{\Delta}_0(v)$, and $\tilde{T}$ at the length scale ξ. To prove this we first note that at the length scale ξ we have $\tilde{\gamma}(v)v=(f-f_c)=\xi^{-1/\nu}$ and therefore $\tilde{\gamma}(v)=v^{-(\nu/\beta)(2-z)}$. Then, by replacing γ by $\tilde{\gamma}(v)$ we get the same velocity and periodicity dependence for l_M and L_M. This justifies the identification of the crossover predicted with the present model with the one from the RM to the RP fast-flow regimes observed in the simulations and estimated in Sec. IV by physical arguments.

B. Elastic string vs elastic chains

We discuss here the equivalence observed between the geometry of an elastic line in a two-dimensional RP potential and the one of a periodic chain in a one-dimensional nonperiodic random potential. We argue that this connection is general between D-dimensional thin interfaces transversely displacing in random-periodic $D+1$-dimensional spaces and a periodic array of $(D-1)$ dimensions coupled interfaces in a D-dimensional random medium. The connection between the two systems is however not trivial since there is no exact mapping between these two systems. We describe first the case of the statics, which can be discussed in terms of the replicated Hamiltonian and complemented with additional transfer-matrix numerical calculations, and then the dynamics.

1. Statics

We start by analyzing first the static problem, i.e., $F=0$ and $T=0$, of the elastic line in a two-dimensional random-periodic disorder and then compare it with that of a one-dimensional elastic chain over a random potential. Let us consider an elastic line described by the univalued function $u(z)$, where u is a function in the transverse direction, and z gives the longitudinal direction. The elastic contribution to the Hamiltonian is

$$H_{\mathrm{e}} = \frac{c}{2}\int dz(\partial_z u)^2 \quad (35)$$

while the disorder contribution in term of the line density $\rho(x,z)$ is

$$H_{\mathrm{dis}} = \int dxdzV(x,z)\rho(x,z). \quad (36)$$

Using the integral representation of the δ function one can write the density as

$$\rho(x,z) = \delta[x-u(z)] = \frac{1}{2\pi}\int d\lambda e^{i\lambda[x-u(z)]}. \quad (37)$$

In order to consider the periodicity of the system in the x direction, the disorder potential can be written as a sum over periodic images as

$$V(x,z) = \sum_p \tilde{V}(x - pM, z), \tag{38}$$

where $\tilde{V}(x,z)$ is the disorder potential defined in the interval $x \in [-M/2, M/2]$. Using this periodic potential one can write for the disorder Hamiltonian that (see the Appendix)

$$H_{\rm dis} = -\frac{\Delta_0}{2TM} \sum_{a,b} \sum_K \int dz e^{-iK[u_a(z) - u_b(z)]}, \tag{39}$$

where $K = 2\pi n/M$. This last expression is strictly identical to the one of a periodic system for which K are the vectors of the reciprocal lattice, as we show in the following.

In order to describe the one-dimensional periodic chain in a one-dimensional disordered potential, let us consider an elastic chain of average lattice space a, which corresponds to average density $\rho_0 = 1/a$. One can imagine a chain composed of masses and springs of constant length. Each "mass" has a finite internal width ω and the center of consecutive masses are separated a distance a. The positions of the particles are given by $x_j = x_j^0 + u_j = ja + u_j$, where $x_j^0 = ja$ is the nominal position in the unperturbed lattice and u_j is the displacement. In order to treat the model one should go from the u_j variables to a continuum formulation. Through this relabeling process, the decomposition of the density in this one-dimensional problem leads to a density field

$$\rho(x) = \sum_j \delta(x - x_j^0 - u_j) \cong \rho_0 \left[1 - \partial_x u(x) + \sum_{K \neq 0} e^{iK[x - u(x)]} \right], \tag{40}$$

where the last expression is valid for $\partial_x u \ll 1$, and $K = 2\pi n/a$ are the reciprocal lattice vectors. The continuum field

$$u(x) = \int_0^{2\pi/a} \frac{dq}{2\pi} e^{iqx} \sum_j e^{iqx_j^0} u_j \tag{41}$$

is valid for $x \gg a$. For details on the relabelling process see Ref. 59, especially Appendix A.

Considering the decomposition of the density and using a replica formalism, the replicated disorder Hamiltonian can be finally written as (see the Appendix)

$$H_{\rm dis} = -\frac{\Delta_c \rho_0^2}{2T} \sum_{ab} \int dx \left[\partial_x u^a(x) \partial_x u^b(x) + \sum_{K \neq 0} e^{-iK[u^a(x) - u^b(x)]} \right], \tag{42}$$

which, with the exception of the $\partial_x u^a(x) \partial_x u^b(x)$ term, is formally equivalent to Eq. (39). However, the original one dimensional chain in a one-dimensional disorder potential, as studied by Cule and Hwa,[51,52] contains also a term proportional to $\partial_x u(x)$. This term is irrelevant at large length scales in dimensions $d > 2$ and gives a finite shift of the correlations function in $d \leq 2$. This term is indeed a renormalization of the quadratic part of the Hamiltonian and it is commonly accepted that it does not change the roughness exponent.[51,52]

Then, when comparing the periodic disorder case to the periodic chain, the period of the disorder potential M becomes the average distance between neighboring particles.

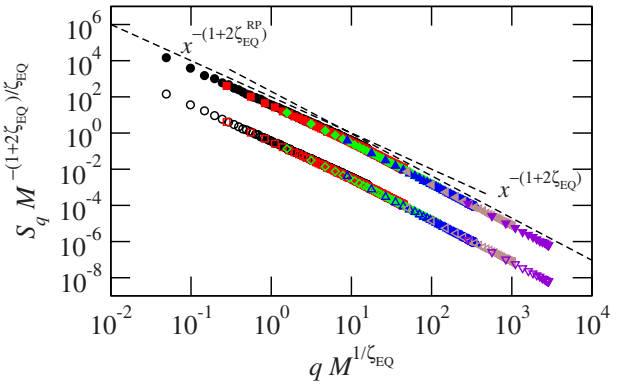

FIG. 9. (Color online) Ground-state geometry of the elastic string (open symbols) and the one-dimensional chain (closed symbols) problems as obtained with transfer matrix calculations. The data are represented in a scaled form and the closed symbols are shifted upwards for clarity.

Thus, when the fluctuation of the particles becomes on the order of the average distance, the system enters a RP or CDW regime. Then, in the static limit, structural fluctuations at large length scales are given by the roughness exponent associated to the static CDW problem, $\zeta_{\rm EQ}^{\rm RP} = 1/2$. At finite $M > 1$ a crossover appears at a given length scale, corresponding to the scale for which the disorder induced fluctuations become of the order of the periodic box.

The geometrical equivalence argued above can be tested directly by transfer-matrix calculations for the ground state of a one-dimensional chain and the one of an elastic string. In Fig. 9 we compare the structure factor of both systems, for different periodicities $M \gg r_f$. We see almost no difference, meaning that the extra terms in the replicated Hamiltonian for the chain are irrelevant. We also find that the structure factor has a crossover at a characteristic length $L_{\rm P}^0 \equiv L_{\rm P}^0(M)$ between a regime with the RM equilibrium roughness exponent $\zeta_{\rm EQ} = 2/3$ at small length scales, to a regime with the RP equilibrium roughness exponent $\zeta_{\rm EQ}^{\rm RP} = 1/2$ at large length scales. In Fig. 9 we show that the structure factor is well described by the scaling formula

$$S_q \sim q^{-(1+2\zeta_{\rm EQ})} \tilde{H}(qL_{\rm P}^0) \tag{43}$$

with a crossover length $L_{\rm P}^0 \sim M^{1/\zeta_{\rm EQ}}$. The function $\tilde{H}(x)$ is such that for small x it behaves as $x^{2(\zeta_{\rm EQ} - \zeta_{\rm EQ}^{\rm RP})}$. The crossover at $L_{\rm P}^0$ can be understood in the same terms as for the crossover length $L_{\rm P}$ at depinning. $L_{\rm P}^0$ is in this case the length at which the width $w(L) \sim L^{\zeta_{\rm EQ}}$ of the interface at the ground state becomes of the order of the periodicity, $w(L_{\rm P}^0) \sim M$. As for depinning when $M \gg r_f$ the structure of the system at equilibrium is identical to the RM one and crosses over to the RP one at large length scales.

2. Dynamics

One can do a similar comparison for the dynamics of the elastic line in the periodic disorder potential and the periodic chain in disordered medium. As usual, we model the motion

of an elastic string in a disordered environment by means of the overdamped equation of motion Eq. (15). The pinning force is

$$F_p = -\frac{\delta H_{\rm dis}}{\delta u_{zt}} = \frac{1}{M}\sum_K \tilde{V}(x,z)(iK)e^{iK(x-u_{zt})}e^{-K^2\omega^2}, \quad (44)$$

where we use the notation $u(z,t) \equiv u_{zt}$. If now one use the Martin-Siggia-Rose formalism as in Ref. 70, then it can be shown that F_p interacts only linearly with the operator $\hat{u}_{zt}$. Thus one can replicate over different times in order to obtain an averaged expression similarly to what was done in the previous section, which results in a term proportional to

$$-\frac{\Delta_0}{M}\sum_K \int dz dt_1 dt_2 K^2 e^{-iK(u_{zt_1}-u_{zt_2})}e^{-2K^2\omega^2}\hat{u}_{zt_1}\hat{u}_{zt_2}. \quad (45)$$

Again, this is equivalent, up to a factor proportional to $\partial_x u(x)$, to the case of the one dimensional periodic system.[70] The main difference is the convective term but it can be shown that it is irrelevant since an arbitrary shift $u(x) \to u(x)+f(x)$ leaves the disorder term unchanged.[70]

C. Roughness diagram in the creep regime

The roughness diagram of Fig. 2 for depinning and the results of Fig. 9 can be combined to infer a roughness diagram as a function of the driving force, including the expected crossovers in the creep regime, $f<f_c$. As it was shown in Ref. 50 for pure RM (or RF) systems, below the depinning threshold f_c a characteristic length $L_{\rm opt} \equiv L_{\rm opt}(f)$ exists. This length grows with decreasing f separating the small length-scales described by the equilibrium ($f=0$) roughness from the depinning ($f=f_c$) roughness. Since $M \gg r_f$, we can expect to observe the same behavior for the random-periodic system at intermediate and small length scales for which the RP systems behave as RM (or RF) systems. Since at large length scales the effect of periodicity should always appear, it is plausible to connect the crossover lengths $L_{\rm P}$ at $f \sim f_c$ and $L_{\rm P}^0$ at $f=0$ by a dynamic crossover length $l_{\rm P} \equiv l_{\rm P}(f,M)$ in the creep regime. The width of the interface at $L_{\rm P}$ is thus given by

$$M \sim (L_{\rm P}^0)^{\zeta_{\rm EQ}} \quad (46)$$

if $f<f_{\rm P}^0$ and

$$M \sim L_{\rm opt}^{\zeta_{\rm EQ}}\left(\frac{l_{\rm P}}{L_{\rm opt}}\right)^{\zeta} \quad (47)$$

if $f_{\rm P}^0<f<f_c$, with $f_{\rm P}^0$ a new characteristic force, defined by the condition $l_{\rm P}(f_{\rm P}^0,M)=L_{\rm P}^0(M)$. Therefore

$$l_{\rm P} \sim L_{\rm opt}\left(\frac{M}{L_{\rm opt}^{\zeta_{\rm EQ}}}\right)^{1/\zeta} \quad (48)$$

with $f_{\rm P}^0<f<f_c$. In the diagram of Fig. 10 we schematically show the crossover length $l_{\rm P}$ separating the RM from the RP depinning roughness in the creep regime. It shows several sectors, including the equilibrium, depinning and fast-flow geometries of both the RM and the RP (note however that the fast flow and depinning RP regimes have the same roughness exponent).

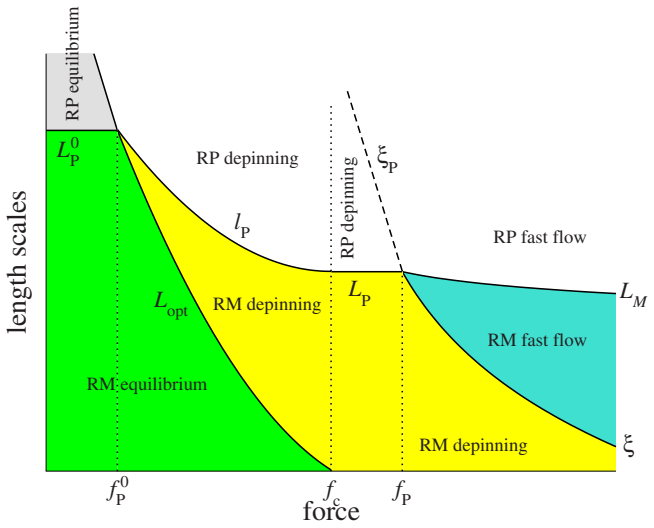

FIG. 10. (Color online) Depinning roughness diagram of Fig. 2 extended to the creep regime $0<f<f_c$, at small temperatures. The diagram displays roughness exponents of the RM and RP classes at equilibrium, depinning, and fast flow.

Note that at variance with L_M, $l_{\rm P}$ can be obtained by a static argument similar to the one used for $L_{\rm P}$ since the velocity vanishes rapidly in the low temperature creep regime. The system has thus enough time to relax all its (nonzero) modes in the time of flight $\tau_M = M/v$. Note in this respect that the largest length scales obey an Edwards-Wilkinson equation with correlated noise, and thus their relaxation times are governed by a dynamic exponent, contrarily to the zero-mode displacement.

D. Periodic boundary conditions and the thermodynamic limit

We present here a discussion concerning numerical simulations and the proper thermodynamic limit. It is well known that when using numerical simulations to describe interface depinning and creep, a main shortcoming of the numerical method is coming from the difficulty in taking the thermodynamic limit $M \to \infty$ and $L \to \infty$. In order to perform a consistent finite-size analysis one has to carefully specify how both M and L should tend to infinity, as different prescriptions for the aspect ratio scaling lead to very different results.

It has been shown that the sample-to-sample fluctuations of the critical force drastically change with the ratio M/L^{ζ}.[62] For very small M compared to L^{ζ} periodicity effects are important and the distribution of critical forces is Gaussian, while at very high values of M the critical force is dominated by extreme values and its distribution becomes of the Gumbel form. In the first case the mean critical force is always bounded while in the latter grows logarithmically with M and is thus infinite in the thermodynamic limit. For the aspect ratio scaling $M \sim L^{\zeta}$ it was shown that the mean critical force is finite and well defined in the thermodynamic limit where the system displays pure RM behavior. In this last case, the critical force distribution is between Gaussian and Gumbel. The aspect ratio scaling $M=kL^{\zeta}$ leaves however open the question of what is the optimal value of k for avoid-

ing effects induced by the transverse boundary conditions. This has motivated the use of a different method for calculating steady-state properties of the same system, in which the control parameter is not the force but the mean velocity of the manifold by replacing the driving force by a uniform spring with constant m^2, $f \to m^2[vt-u(\mathbf{r})]$, pulling the whole manifold at a constant speed v in a transversely infinite medium. This model allows for more direct comparisons with analytical calculations,[48,71–76] and has the advantage, compared with the force-controlled model, that the characteristic length L_m induced by the parabolic moving potential is controlled only by the spring constant $L_m \sim 1/m$, and not by the velocity-dependent geometry of the manifold. When modeling a system for which the spring has not a physical origin the correct scaling for the spring constant is simply $L_m \sim L$ in this case and thus very small values of m are required in the large-scale limit.

If one wants to stick to the constant-force model the most natural empirical choice for the aspect ratio scaling is $w(L) \approx M$, where w is the average width of the manifold.[62] The problem with such prescription is that $w(L)$, being an integrated quantity $w \sim \int dq S_q$, has a complicate dependence with the mean velocity of the manifold through the velocity-dependent correlations lengths separating different regimes of roughness, and through the values of the different roughness exponents. The geometrical roughness diagram of Fig. 2 shows clearly that this is indeed the case, and gives at the same time an answer to this problem. It shows that for a fixed value of M, the optimal aspect ratio scalings are $L = L_{\mathrm{P}}(M)$ for $v < v_{\mathrm{P}}$, equivalent to those proposed in Ref. 62, but a different aspect-ratio scaling, $L = L_M(v,M)$, for $v > v_{\mathrm{P}}$. Figure 2 thus shows that using a velocity-independent prescription $L = L_{\mathrm{P}}(M) \sim M^{1/\zeta}$, which works for the critical configuration, would always give inconsistent results at all nonzero velocities in the thermodynamic limit, since $v_{\mathrm{P}} \to 0$ when $M \to \infty$ and then $L \gg L_M$ at a fixed v. Therefore, by increasing M within this prescription the system would eventually display periodicity induced effects at any finite v, inducing an artificial crossover as a function of the velocity in nonperiodic systems. This crossover induced by periodicity is on the other hand physically interesting for RP systems with localized correlation peaks.

VIII. CONCLUSIONS

We have studied numerically the depinning transition of driven elastic interfaces in a random-periodic medium with localized periodic-correlation peaks in the direction of motion. We have obtained a dynamical roughness diagram which contains, at small length scales, the critical and fast-flow regimes typical of the RM (or domain wall) depinning, and at large length scales, the critical and fast-flow regimes typical of the RP (or charge-density wave) depinning. From the equilibrium behavior of these kind of systems we have also inferred a richer dynamical roughness diagram including the low-temperature creep regime which additionally includes roughness sectors corresponding to the equilibrium geometry of the RP and RM classes.

Our results are relevant for understanding the geometry at depinning of periodic arrays of elastically coupled thin manifolds in a disordered medium such as driven particle chains or vortex-line planar arrays since these periodic systems display localized periodic correlation peaks. In particular, our results are relevant for properly controlling the effect of transverse periodic boundary conditions in large-scale simulations of constant-force driven disordered interfaces. From the roughness diagrams of Figs. 2 and 10 we see indeed that the aspect ratio relation must be carefully chosen when taking the thermodynamic limit, depending whether one wants to study the large-scale behavior of a pure RM or a RP system.

We have also argued that there is a geometrical equivalence between the d-dimensional periodic elastic system moving in d dimensions and the d-dimensional elastic interface moving in a $d+1$ dimensional periodic medium, although the mapping between these two systems is not exact. In this respect we note that the $d=1$ case we have studied numerically is the most stringent case since it goes beyond the usual small slope approximation used to develop the density in periodic components, Eq. (40). Indeed, since the roughness exponent for chains is larger than one, the average difference between the displacements of neighboring particles grows with the system size, violating the small slope approximation for large systems. Despite this fact, the results still remain valid even for the one dimensional case. We thus conclude that this equivalence is rather robust and should hold for higher dimensional cases.

ACKNOWLEDGMENTS

This work was supported in part by the Swiss National Science Foundation under MaNEP and Division II. S.B. and A.B.K. acknowledge financial support from ANPCyT under Grant No. PICT2007886 and CONICET under Grant No. PIP11220090100051.

APPENDIX: ELASTIC STRING VS ELASTIC CHAINS

In this appendix we show how the disorder Hamiltonian for the elastic string in periodic disorder and for the periodic chain in one-dimensional disorder can be obtained.

1. Two-dimensional periodic disorder

The disorder contribution to the full Hamiltonian of the system is

$$H_{\mathrm{dis}} = \int dx dz V(x,z)\rho(x,z). \tag{A1}$$

The line density $\rho(x,z)$ gives the position of the interface.

In order to consider the periodicity of the system in the x direction, the disorder potential can be written as a sum over periodic images as

$$V(x,z) = \sum_p \tilde{V}(x - pM, z), \tag{A2}$$

where $\tilde{V}(x,z)$ is the disorder potential defined in the interval $x \in [-M/2, M/2]$. In terms of a traditional uncorrelated Gaussian disorder $V_0(x,z)$, one can directly define

$$\tilde{V}(x,z) = \Theta_M(x,z) V_0(x,z) \tag{A3}$$

using that

$$\Theta_M(x,z) = \begin{cases} 1 & \text{if } x \in [-M/2, M/2] \\ 0 & \text{otherwise.} \end{cases} \tag{A4}$$

The disorder term thus becomes

$$H_{\text{dis}} = \int dx dz V(x,z) \delta[x - u(z)]$$
$$= \int dx dz \Theta_M(x,z) V_0(x,z) \sum_p \delta[x - pM - u(z)]. \tag{A5}$$

In order to obtain a disorder averaged Hamiltonian we use the replica trick[59,77]

$$H_{\text{dis}} = -\frac{1}{2T} \sum_{ab} \int dx dx' \overline{V(x)V(x')} \rho_a(x) \rho_b(x'). \tag{A6}$$

Then, using the integral representation of the δ function

$$\rho(x,z) = \delta[x - u(z)] = \frac{1}{2\pi} \int d\lambda e^{i\lambda[x-u(z)]} \tag{A7}$$

the replicated Hamiltonian reads[59]

$$H_{\text{dis}} = -\frac{1}{2T} \sum_{a,b} \sum_{p_1,p_2} \int dx_1 dz_1 dx_2 dz_2 \Theta_M(x_1,z_1) \Theta_M(x_2,z_2)$$
$$\times \overline{V_0(x_1,z_1) V_0(x_2,z_2)}$$
$$\times \delta[x_1 - p_1 M - u_a(z_1)] \delta[x_2 - p_2 M - u_b(z_2)]. \tag{A8}$$

Now, using for the disorder potential correlator that

$$\overline{V_0(x_1,z_1) V_0(x_2,z_2)} = \Delta_0 \delta(x_1 - x_2) \delta(z_1 - z_2) \tag{A9}$$

and since $\Theta_M = 0,1$ implies $\Theta_M^2 = \Theta_M$, one has

$$H_{\text{dis}} = -\frac{\Delta_0}{2T} \sum_{a,b} \sum_{p_1,p_2} \int dx dz \Theta_M(x,z)$$
$$\times \delta[x - p_1 M - u_a(z)] \delta[x - p_2 M - u_b(z)]. \tag{A10}$$

Now, we perform the sum over the localization function, resulting in

$$\sum_{p_1} \delta[x - p_1 M - u_a(z)] = \frac{1}{M} \sum_{K_1} e^{iK_1[x-u_a(z)]}, \tag{A11}$$

where $K_1 = 2\pi n_1 / M$ and we used that

$$\sum_j e^{iqjM} = \frac{2\pi}{M} \sum_K \delta(q - K). \tag{A12}$$

Thus, the disorder Hamiltonian can now be written as

$$H_{\text{dis}} = -\frac{\Delta_0}{2TM^2} \sum_{a,b} \sum_{K_1,K_2} \int dx dz \Theta_M(x,z)$$
$$\times e^{iK_1[x-u_a(z)]} e^{iK_2[x-u_b(z)]}. \tag{A13}$$

Now, using that

$$\int_{-M/2}^{M/2} dx e^{i(K_1 - K_2)x} = M \delta_{K_1,K_2} \tag{A14}$$

performing the integral over x and summing over K_2, one arrives at

$$H_{\text{dis}} = -\frac{\Delta_0}{2TM} \sum_{a,b} \sum_K \int dz e^{-iK[u_a(z) - u_b(z)]}. \tag{A15}$$

2. One-dimensional periodic chain

The positions of the particles are given by $x_j = x_j^0 + u_j = ja + u_j$, where $x_j^0 = ja$ is the nominal position in the unperturbed lattice, u_j is the displacement and a is the average lattice space. In order to treat the model one should go from the u_j variables to a continuum formulation. Through this relabelling process, the decomposition of the density in this one-dimensional problem leads to a density field

$$\rho(x) = \sum_j \delta(x - x_j^0 - u_j) \cong \rho_0 \left[1 - \partial_x u(x) + \sum_{K \neq 0} e^{iK[x-u(x)]} \right], \tag{A16}$$

where the last expression is valid for $\partial_x u \ll 1$, $K = 2\pi n / a$, and the continuum field

$$u(x) = \int_0^{2\pi/a} \frac{dq}{2\pi} e^{iqx} \sum_j e^{iqx_j^0} u_j \tag{A17}$$

is valid for $x \gg a$. This relabelling process is carefully described in Ref. 59, especially Appendix A, and we refer the interested reader to this work.

Considering the decomposition of the density, the Hamiltonian part corresponding to the uncorrelated Gaussian disorder $V_c(x)$ with $\overline{V_c(x)V_c(x')} = \Delta_c \delta(x - x')$ is

$$H_{\text{dis}} = \int dx V_c(x) \rho(x)$$
$$\cong \rho_0 \int dx V_c(x) \left[1 - \partial_x u(x) + \sum_{K \neq 0} e^{iK[x-u(x)]} \right]. \tag{A18}$$

When replicating the Hamiltonian one has

$$H_{\text{dis}} = -\frac{\Delta_c \rho_0^2}{2T} \sum_{ab} \int dx \left[1 - \partial_x u^a(x) - \partial_x u^b(x) + \sum_{K \neq 0} e^{iK[x-u^a(x)]} \right.$$
$$+ \sum_{K' \neq 0} e^{iK'[x-u^b(x)]} + \partial_x u^a(x) \partial_x u^b(x)$$
$$\left. - \partial_x u^a(x) \sum_{K' \neq 0} e^{iK'[x-u^b(x)]} - \partial_x u^b(x) \sum_{K \neq 0} e^{iK[x-u^a(x)]} \right]$$

$$+ \sum_{K,K' \neq 0} e^{-x(K+K')} e^{-i[Ku^a(x)+K'u^b(x)]} \Bigg]. \quad \text{(A19)}$$

In this last expression one should drop constant shift terms and rapidly oscillating terms. Then, setting $K=-K'$ in this last expression one has

$$H_{\text{dis}} = -\frac{\Delta_c \rho_0^2}{2T} \sum_{ab} \int dx \left[\partial_x u^a(x) \partial_x u^b(x) + \sum_{K \neq 0} e^{-iK[u^a(x)-u^b(x)]} \right]. \quad \text{(A20)}$$

[1] S. Lemerle, J. Ferré, C. Chappert, V. Mathet, T. Giamarchi, and P. Le Doussal, Phys. Rev. Lett. **80**, 849 (1998).
[2] M. Bauer, A. Mougin, J. P. Jamet, V. Repain, J. Ferré, R. L. Stamps, H. Bernas, and C. Chappert, Phys. Rev. Lett. **94**, 207211 (2005).
[3] M. Yamanouchi, D. Chiba, F. Matsukura, T. Dietl, and H. Ohno, Phys. Rev. Lett. **96**, 096601 (2006).
[4] P. J. Metaxas, J. P. Jamet, A. Mougin, M. Cormier, J. Ferré, V. Baltz, B. Rodmacq, B. Dieny, and R. L. Stamps, Phys. Rev. Lett. **99**, 217208 (2007).
[5] P. Paruch, T. Giamarchi, and J. M. Triscone, Phys. Rev. Lett. **94**, 197601 (2005).
[6] P. Paruch and J. M. Triscone, Appl. Phys. Lett. **88**, 162907 (2006).
[7] W. Kleemann, Annu. Rev. Mater. Res. **37**, 415 (2007).
[8] S. Moulinet, A. Rosso, W. Krauth, and E. Rolley, Phys. Rev. E **69**, 035103(R) (2004).
[9] P. Le Doussal, K. J. Wiese, S. Moulinet, and E. Rolley, Europhys. Lett. **87**, 56001 (2009).
[10] N. Martys, M. Cieplak, and M. O. Robbins, Phys. Rev. Lett. **66**, 1058 (1991).
[11] I. Hecht and H. Taitelbaum, Phys. Rev. E **70**, 046307 (2004).
[12] E. Bouchaud, J. P. Bouchaud, D. S. Fisher, S. Ramanathan, and J. R. Rice, J. Mech. Phys. Solids **50**, 1703 (2002).
[13] M. Alava, P. K. V. V. Nukalaz, and S. Zapperi, Adv. Phys. **55**, 349 (2006).
[14] D. Bonamy, S. Santucci, and L. Ponson, Phys. Rev. Lett. **101**, 045501 (2008).
[15] L. Ponson, Phys. Rev. Lett. **103**, 055501 (2009).
[16] L. Ponson, D. Bonamy, and E. Bouchaud, Phys. Rev. Lett. **96**, 035506 (2006).
[17] T. Nattermann and S. Brazovskii, Adv. Phys. **53**, 177 (2004).
[18] G. Blatter, M. V. Feigel'man, V. B. Geshkenbein, A. I. Larkin, and V. M. Vinokur, Rev. Mod. Phys. **66**, 1125 (1994).
[19] T. Giamarchi and S. Bhattacharya, in *High Magnetic Fields: Applications in Condensed Matter Physics and Spectroscopy*, Lecture Notes in Physics, edited by C. Berthier, L. P. Lévy, G. Martinez (Springer-Verlag, Berlin, 2002) p. 314.
[20] X. Du, G. Li, E. Y. Andrei, M. Greenblatt, and P. Shuk, Nat. Phys. **3**, 111 (2007).
[21] T. Giamarchi, in *Quantum Phenomena in Mesoscopic Systems*, Proceedings of the International School of Physics "Enrico Fermi" (IOS Press, Bologna, 2003).
[22] A. I. Larkin and Y. N. Ovchinnikov, J. Low Temp. Phys. **34**, 409 (1979).
[23] M. Kardar, Phys. Rep. **301**, 85 (1998).
[24] D. S. Fisher, Phys. Rep. **301**, 113 (1998).
[25] L. B. Ioffe and V. M. Vinokur, J. Phys. C **20**, 6149 (1987).
[26] T. Nattermann, Europhys. Lett. **4**, 1241 (1987).
[27] A. A. Middleton, Phys. Rev. B **45**, 9465 (1992).
[28] D. S. Fisher, Phys. Rev. B **31**, 1396 (1985).
[29] P. Le Doussal, K. J. Wiese, and P. Chauve, Phys. Rev. B **66**, 174201 (2002).
[30] O. Narayan and D. S. Fisher, Phys. Rev. B **46**, 11520 (1992).
[31] T. Nattermann, S. Stepanow, L. H. Tang, and H. Leschhorn, J. Phys. II **2**, 1483 (1992).
[32] P. Chauve, T. Giamarchi, and P. Le Doussal, Europhys. Lett. **44**, 110 (1998).
[33] P. Chauve, T. Giamarchi, and P. Le Doussal, Phys. Rev. B **62**, 6241 (2000).
[34] L. W. Chen and M. C. Marchetti, Phys. Rev. B **51**, 6296 (1995).
[35] D. Vandembroucq, R. Skoe, and S. Roux, Phys. Rev. E **70**, 051101 (2004).
[36] U. Nowak and K. D. Usadel, Europhys. Lett. **44**, 634 (1998).
[37] L. Roters, A. Hucht, S. Lübeck, U. Nowak, and K. D. Usadel, Phys. Rev. E **60**, 5202 (1999).
[38] L. Roters, S. Lübeck, and K. D. Usadel, Phys. Rev. E **66**, 069901(E) (2002).
[39] A. Rosso and W. Krauth, Phys. Rev. Lett. **87**, 187002 (2001).
[40] A. Rosso and W. Krauth, Phys. Rev. E **65**, 025101(R) (2002).
[41] A. Rosso, A. K. Hartmann, and W. Krauth, Phys. Rev. E **67**, 021602 (2003).
[42] O. Duemmer and W. Krauth, Phys. Rev. E **71**, 061601 (2005).
[43] S. Bustingorry, A. B. Kolton, and T. Giamarchi, Europhys. Lett. **81**, 26005 (2008).
[44] A. A. Middleton, Phys. Rev. Lett. **68**, 670 (1992).
[45] D. S. Fisher, Phys. Rev. Lett. **56**, 1964 (1986).
[46] L. Balents and D. S. Fisher, Phys. Rev. B **48**, 5949 (1993).
[47] A. B. Kolton, A. Rosso, E. V. Albano, and T. Giamarchi, Phys. Rev. B **74**, 140201 (2006).
[48] A. Rosso, P. Le Doussal, and K. J. Wiese, Phys. Rev. B **75**, 220201(R) (2007).
[49] A. B. Kolton, A. Rosso, T. Giamarchi, and W. Krauth, Phys. Rev. Lett. **97**, 057001 (2006).
[50] A. B. Kolton, A. Rosso, T. Giamarchi, and W. Krauth, Phys. Rev. B **79**, 184207 (2009).
[51] D. Cule and T. Hwa, Phys. Rev. Lett. **77**, 278 (1996).
[52] D. Cule and T. Hwa, Phys. Rev. B **57**, 8235 (1998).
[53] L.-H. Tang, M. Kardar, and D. Dhar, Phys. Rev. Lett. **74**, 920 (1995).
[54] A. A. Fedorenko, P. Le Doussal, and K. J. Wiese, Phys. Rev. E **74**, 061109 (2006).
[55] H. Fukuyama and P. A. Lee, Phys. Rev. B **17**, 535 (1978).
[56] P. A. Lee and T. M. Rice, Phys. Rev. B **19**, 3970 (1979).
[57] R. Chitra, T. Giamarchi, and P. Le Doussal, Phys. Rev. B **65**, 35312 (2001).
[58] T. Giamarchi and P. Le Doussal, Phys. Rev. Lett. **72**, 1530 (1994).

[59] T. Giamarchi and P. Le Doussal, Phys. Rev. B **52**, 1242 (1995).
[60] P. Kim, Z. Yao, C. A. Bolle, and C. M. Lieber, Phys. Rev. B **60**, R12589 (1999).
[61] M. I. Dolz, A. B. Kolton, and H. Pastoriza, Phys. Rev. B **81**, 092502 (2010).
[62] C. J. Bolech and A. Rosso, Phys. Rev. Lett. **93**, 125701 (2004).
[63] A. B. Kolton, A. Rosso, and T. Giamarchi, Phys. Rev. Lett. **94**, 047002 (2005).
[64] A. B. Kolton, A. Rosso, and T. Giamarchi, Phys. Rev. Lett. **95**, 180604 (2005).
[65] S. F. Edwards and D. R. Wilkinson, Proc. R. Soc. London, Ser. A **381**, 17 (1982).
[66] A. Rosso and W. Krauth, Phys. Rev. B **65**, 012202 (2001).
[67] H. J. Jensen, J. Phys. A **28**, 1861 (1995).
[68] P. Le Doussal (private communication).
[69] A. E. Koshelev and V. M. Vinokur, Phys. Rev. Lett. **73**, 3580 (1994).
[70] P. Le Doussal and T. Giamarchi, Phys. Rev. B **57**, 11356 (1998).
[71] P. Le Doussal, A. A. Middleton, and K. J. Wiese, Phys. Rev. E **79**, 050101 (2009).
[72] P. Le Doussal and K. J. Wiese, Europhys. Lett. **77**, 66001 (2007).
[73] A. A. Middleton, P. Le Doussal, and K. J. Wiese, Phys. Rev. Lett. **98**, 155701 (2007).
[74] P. Le Doussal and K. J. Wiese, Phys. Rev. E **79**, 051105 (2009).
[75] P. Le Doussal and K. J. Wiese, Phys. Rev. E **79**, 051106 (2009).
[76] A. Rosso, P. Le Doussal, and K. J. Wiese, Phys. Rev. B **80**, 144204 (2009).
[77] M. Mézard and G. Parisi, J. Phys. I **1**, 809 (1991).